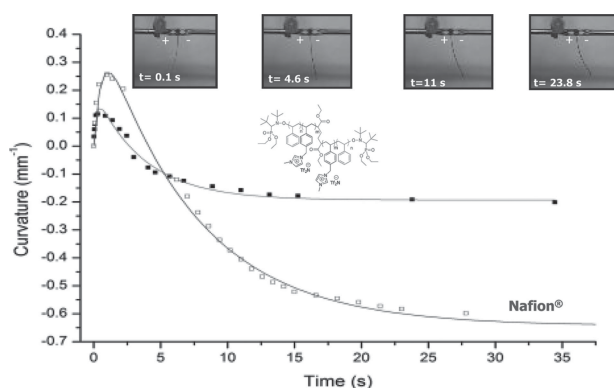


# Well-Defined Imidazolium ABA Triblock Copolymers as Ionic-Liquid-Containing Electroactive Membranes

Chainika Jangu, Jing-Han Helen Wang, Dong Wang, Sharon Sharick, James R. Heflin, Karen I. Winey, Ralph H. Colby, Timothy E. Long\*

Nitroxide-mediated polymerization (NMP) affords the synthesis of well-defined ABA triblock copolymers with polystyrene external blocks and a charged poly(1-methyl-3-(4-vinylbenzyl)-imidazolium bis(trifluoromethane sulfonyl)imide central block. Aqueous size-exclusion chromatography (SEC) and  $^1\text{H}$  NMR spectroscopy studies confirm the control of the composition and block lengths for both the central and external blocks. Dynamic mechanical analysis (DMA) reveals a room temperature modulus suitable for fabricating these triblock copolymers into electroactive devices in the presence of an added ionic liquid. Dielectric relaxation spectroscopy (DRS) elucidates the ion-transport properties of the ABA triblock copolymers with varied compositions. The ionic conductivity in these single-ion conductors exhibits Vogel–Fulcher–Tammann (VFT) and Arrhenius temperature dependences, and electrode polarization (EP) analysis determines the number density of simultaneously conducting ions and their mobility. The actuators derived from these triblock copolymer membranes experience similar actuation speeds at an applied voltage of 4 V DC, as compared with benchmark Nafion membranes. These tailorable ABA block copolymers are promising candidates for ionic-polymer device applications.



C. Jangu, Prof. T. E. Long  
Department of Chemistry, Macromolecules and Interfaces  
Institute, Virginia Tech., Blacksburg, VA 24061, USA  
E-mail: telong@vt.edu

J.-H. H. Wang, Prof. R. H. Colby  
Department of Chemical Engineering, The Pennsylvania State  
University, University Park, PA 16802, USA

D. Wang, Prof. J. R. Heflin  
Department of Physics, Virginia Tech., Blacksburg, VA 24061,  
USA

S. Sharick, Prof. K. I. Winey  
Department of Materials Science and Engineering, University  
of Pennsylvania, Philadelphia, PA 19104, USA

## 1. Introduction

Electroactive polymers (EAPs) have attracted significant attention in the last decade.<sup>[1–5]</sup> EAPs potentially enable large strains (>1%) at low applied voltages (<10 V)<sup>[1]</sup> and involve multiple physical processes such as electrostatic interaction between charged electrodes, generated stress upon the application of an electric field, and ion-transport and charge accumulation to facilitate electromechanical coupling.<sup>[1,6,7]</sup> Ion-containing polymeric membranes form a class of devices classified as ionic-polymer transducers, and these electromechanical transducers enable potential

applications including sensors and actuators, energy-harvesting devices, and biomimetic materials.<sup>[8,9]</sup> For example, an electromechanical actuator typically consists of an ionic polymeric membrane with conductive network composite (CNC) layers and external electrodes coated on both sides. The CNC is often fabricated through layer-by-layer (LbL) self-assembly using positively charged poly(allylamine) hydrochloride and anionic gold nanoparticles.<sup>[10–12]</sup> The CNC layers serve to increase the interfacial surface area and porosity of the electrode, which improves ion-transport and ion accumulation, leading to improved performance of actuation.<sup>[1,9,13,14]</sup>

The most widely studied ionic polymer for transducer membranes is Nafion, serving as a benchmark for optimized properties and response required for the preparation of electromechanical transducers.<sup>[15,16]</sup> A microphase-separated morphology contributes to superior performance as a transducer, i.e., the semicrystalline-perfluorinated backbone provides mechanical stability, and perfluorinated polyether side chains terminated with sulfonic acid groups enable ion (proton) conduction. This multiphase morphology provides an ion-cluster morphology and ion channels upon hydration.<sup>[17,18]</sup> The synthesis of ABA triblock copolymer architectures is an attractive strategy to mimic the morphology of Nafion, where the external blocks provide mechanical reinforcement and an ion-rich central block facilitates ion migration.<sup>[19]</sup> The previous literature describes the tuning of thermomechanical properties, morphology, and ionic conductivity for electroactive membrane applications.<sup>[12,20]</sup> However, a detailed study of charged ABA triblock copolymers with intentionally added ionic liquid remains unprecedented. The charged ABA triblock copolymer serves to localize the ionic liquid electrolyte at the nanometer dimension.

Tuning ABA triblock composition enables tailored charge content, mechanical properties, and morphology.<sup>[21,22]</sup> The interplay between glass transition temperature ( $T_g$ ) and ionic conductivity is firmly described in the literature, and recent studies focused on the influence of diblock copolymer morphology on ionic conductivity.<sup>[22–24]</sup> The triblock copolymers provided suitable mechanical properties for device fabrication; however, fundamental studies of the influence of composition on morphology and ion-transport remain deficient. A significant disadvantage of commercially available polymers for electromechanical transducers is the lack of rational synthetic design of many parameters such as thermomechanical properties, morphology, molecular weight, and composition.

The self-assembled, nanostructured morphologies of block copolymers enable their use as solid-state polyelectrolytes, specifically tuning morphology to benefit ion-transport. A recent report on charged block copolymers demonstrated that morphology is dependent on both

composition and film-processing conditions, and these differences in morphology had a significant impact on ionic conductivity. Elabd et al. demonstrated a two-order increase in ionic conductivity from random copolymers to block copolymers.<sup>[25]</sup> Our group has also reported the synthesis of high-molecular-weight poly[Sty-*b*-(*n*BMA-co-DMAEMA)-*b*-Sty] ABA triblock copolymers using RAFT methods, and triblock copolymers with added ionic liquid showed electro-responsiveness under the application of a low voltage (2–4 V).<sup>[11]</sup>

Our research group has described ABA triblock copolymers using nitroxide-mediated polymerization (NMP) of polystyrene external blocks and a charged imidazolium-containing central block.<sup>[12]</sup> These triblock copolymers exhibited sufficient modulus and ionic conductivity for electromechanical transducers; however, the synthetic consequence of homopolymer central block and diblock copolymer contamination limited long-range order of microphase separation and prevented precise formation as observed in small-angle X-ray scattering (SAXS).<sup>[12]</sup> Also, earlier efforts did not report actuation behavior in the presence of added ionic liquid.

This manuscript will investigate cationic imidazole-containing ABA triblock copolymers that mimic the combined mechanical properties and ion conductivity of commercially available Nafion with comparable actuation performance. NMP was successfully used to obtain targeted molecular weight and tunable compositions. The manuscript will describe novel ABA triblock copolymers with optimized conditions for quaternization and anion-exchange reactions as compared to earlier reported results to obtain well-defined triblock copolymers with narrow PDIs. Thermomechanical properties displayed microphase-separation and a modulus suitable for device fabrication. Dielectric relaxation spectroscopy (DRS) determined ion-transport properties of these charged ABA triblock copolymers with different compositions. The electrode polarization (EP) model provided ionic mobility, dielectric constant, and mobile ion concentration for these triblock copolymer systems. Furthermore, these triblock copolymers with suitable morphology and modulus were cast into ductile films with ionic liquid and fabricated into electromechanical actuators. These ABA triblock copolymers show actuation behavior in the presence of ionic liquid for the first time in the literature.

## 2. Experimental Section

### 2.1. Materials

4-Vinylbenzyl chloride (VBCl) (90%; Sigma) and imidazole (99%; Sigma), 1-bromoethane (98%; Sigma), sodium bicarbonate (>99.5%; Sigma), sodium acetate (>99%; Sigma), sodium

hydroxide (>98%; Sigma), glacial acetic acid (>99%; Sigma), hydrochloric acid (37%; Sigma), 1-ethyl-3-methylimidazolium trifluoromethane sulfonate (EMIm-TfO) (99%; IoLiTec Inc.), and lithium bis(trifluoromethane sulfonyl)imide (Tf<sub>2</sub>N) (LiTf<sub>2</sub>N) (99%; Aldrich) were used as received. Styrene (99%; Sigma) was passed over silica to remove inhibitor prior to use. Acetone (high-performance liquid chromatography (HPLC) grade; Fisher Scientific), ethyl acetate (HPLC grade; Fisher Scientific), diethyl ether (American Chemical Society (ACS) grade; Fisher Scientific), methanol (HPLC grade; Fisher Scientific), hexanes (HPLC grade; Fisher Scientific), and *N,N*-dimethylformamide (DMF) (Fisher Scientific) were used as received. DEPN and DEPN<sub>2</sub> were synthesized according to procedures described in the literature.<sup>[26–28]</sup>

## 2.2. Analytical Methods

<sup>1</sup>H NMR spectroscopy was performed using a 400 MHz Varian Unity at 25 °C. Thermogravimetric analysis (TGA) was performed using a TA Instruments TGA 2950 at a 10 °C min<sup>-1</sup> heating ramp. Differential scanning calorimetry (DSC) was performed using a TA Instruments Q1000. Scans were obtained under N<sub>2</sub> with heating at 10 °C min<sup>-1</sup> and cooling at 100 °C min<sup>-1</sup>; T<sub>g</sub>s were recorded on the second heating cycle. Dynamic mechanical analysis (DMA) was performed with a TA Instruments Q800 at a 3 °C min<sup>-1</sup> heating ramp in film tension mode, and a single frequency of 1 Hz. Aqueous size-exclusion chromatography (SEC) in a ternary mixture of water, methanol, and acetic acid (54:23:23 v/v/v%) with 0.1 M sodium acetate at 35 °C, and a flow rate of 0.8 mL min<sup>-1</sup>, determined the absolute weight-average molecular weights ( $\bar{M}_w$ ) using the refractive index detector and a multi-angle laser light scattering (MALLS) detector. Poly(1-(4-vinylbenzyl)imidazole) neutral as well as charged homopolymers (1.0 mg mL<sup>-1</sup>) was dissolved in the ternary mixture and injected into the dRI detector with a syringe pump. Refractive index increment ( $dn/dc$ ) measurements were performed using a Wyatt Optilab T-rEX equipped with a 690 nm laser at 35 °C. The  $dn/dc$  values were determined with the Astra V software from Wyatt for the determination of absolute  $\bar{M}_w$  from SEC.

Samples for DRS measurements were solvent-cast films from mixtures of 80:20 CHCl<sub>3</sub>:CH<sub>3</sub>OH and vacuum annealed for 5 d at 120 °C. Samples were then placed on a freshly polished brass electrode and dried in a vacuo at 353 K for 48 h and finally a second brass electrode was placed on top of the sample. A Novocontrol GmbH Concept 40 broadband dielectric spectrometer measured the dielectric permittivity. Frequency sweeps were performed isothermally from 10 MHz to 0.01 Hz, in the temperature range from 233 to 453 K under dry nitrogen. The samples were initially held at a temperature above 393 K for at least 30 min to minimize the amount of water and avoid a change in water content during the experiment. The measurements were performed during subsequent cooling under a flow of dry N<sub>2</sub>, and the sample was subsequently heated to the starting temperature, revealing that data are perfectly reproducible during the second heating to the highest temperature.

SAXS was performed on a multi-angle X-ray scattering system, which generates Cu-K<sub>α</sub> X-rays,  $\lambda = 0.154$  nm, from a Nonius FR 591 rotating anode operated at 40 kV and 85 mA. The bright, highly collimated beam was obtained via Osmic Max-Flux optics and pinhole collimation in an integral vacuum system. The scattering

data were collected using a Bruker Hi-Star 2D detector with a sample-to-detector distance of 150 cm. Room-temperature data were collected along the through-plane direction for 1 h. Data were analyzed using Datasqueeze software.<sup>[29]</sup> The intensities were first corrected for primary beam intensity and background scattering was subsequently subtracted. The isotropic 2D scattering patterns were then azimuthally integrated to yield 1D intensity versus scattering vector ( $q$ ) profiles. The intensities were reported in arbitrary units (a.u.).

The LbL fabrication process is identical to our previous publications,<sup>[12,30,31]</sup> where negatively charged gold nanoparticles (3 nm diameter, 20 ppm, Purest Colloids) are deposited LbL with positively charged inert long-chain polyelectrolyte ( $10 \times 10^{-3}$  M poly(allylamine hydrochloride) (PAH) (Sigma–Aldrich). The highly conductive and porous CNC layers within the actuator provided extra volume for ion accumulation and thus enhance the bending performance of the actuator. After hot-pressing (80 °C, 500 lbs) with 50 nm thick gold foil on both sides as electrodes to the power supply, the membrane was cut into 1 mm × 1 cm strips for testing. 4V DC step input was applied to the actuator and a high definition camera recorded bending. As a reference, Nafion-based actuators were fabricated by coating 30 BLs CNC on both sides of the membrane and soaking in EMI-TfO IL to 35 wt% uptake. The same gold foil was hot-pressed under 90 °C, 700 psi. The membrane was cut into strips and tested under identical conditions.

## 2.3. Synthesis of Poly(VBIm)

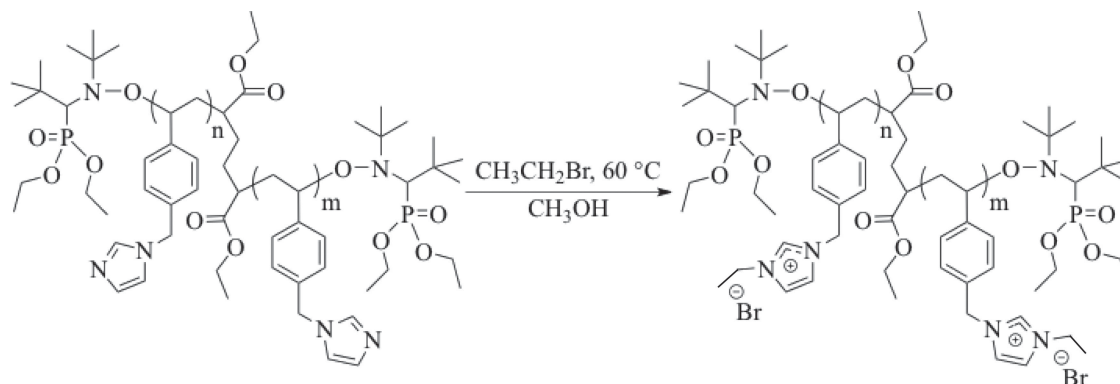
As an example, VBIm (20.6966 g, 112.3 mol), DEPN<sub>2</sub> (135.6 mg, 0.17 mmol), and DEPN (11.3 mg, 0.03 mmol) were synthesized as our previously published procedure,<sup>[9,12,26,28]</sup> and dissolved in DMF (25 mL) and degassed using three freeze–pump–thaw cycles. The flask was back-filled with argon and heated to 125 °C for 2 h. The solution was cooled to 23 °C, diluted with DMF (20 mL), and precipitated into ethyl acetate. The product was redissolved in methanol and precipitated into diethyl ether. Poly(VBIm) was filtered and dried at reduced pressure (0.5 mm Hg) at 40 °C for 18 h. Molecular weight increased linearly with conversion and the PDIs remained narrow (<1.1) throughout the polymerization. SEC chromatographs shifted to lower elution times with increasing polymerization time or conversion.

## 2.4. Quaternization of Poly(VBIm)

Poly(VBIm) and alkyl halide, either 1-bromoethane or methyl iodide, were dissolved in methanol. The solution was purged with argon, and heated to 60 °C with 1-bromoethane and at 23 °C with methyl iodide for 18 h as shown in Scheme 1. The solution was cooled to 23 °C and the product was precipitated into ethyl acetate. Poly(EVBIm-Br) or poly (MVBIm-I) was isolated through filtration and dried under reduced pressure (0.5 mmHg) at 40 °C for 18 h.

## 2.5. Anion Exchange

Poly(EVBIm-Br) (14.8135 g, 50.5 mmol of repeat unit) or poly (MVBIm-I) and LiTf<sub>2</sub>N (72.0395 g, 0.250 mol) were dissolved in separate solutions of water (50 mL each). The solutions were



■ Scheme 1. Quaternization of poly(VBIm) using 1-bromoethane at 60 °C.

mixed together, immediately forming a white precipitate, and stirred at 23 °C for 24 h as shown in Scheme 2. Poly(EVBIm-Tf<sub>2</sub>N) or poly(MVBIm-Tf<sub>2</sub>N) was dialyzed against methanol for 3 d to ensure removal of ionic impurities from the central block.

## 2.6. Chain Extension of Poly(EVBIm-Br-20 °C)

To confirm controlled polymerization, poly(EVBIm-Tf<sub>2</sub>N) (9.2 × 10<sup>-6</sup> mol), VBIm (10.1415 g, 97.3 mmol), and DEPN (4.0 mg, 0.01 mmol) were dissolved in DMF (17.2 mL). The solution was degassed using three freeze–pump–thaw cycles and back-filled with argon. The solution was then heated to 125 °C for polymerization shown in Scheme 3. The solution was cooled to 23 °C, diluted with acetone (50 mL), and precipitated into hexanes. Poly[Sty-*b*-(MVBIm)(Tf<sub>2</sub>N)-*b*-Sty] was isolated through filtration and dried at reduced pressure (0.5 mm Hg) at 40 °C for 18 h.

## 3. Results and Discussion

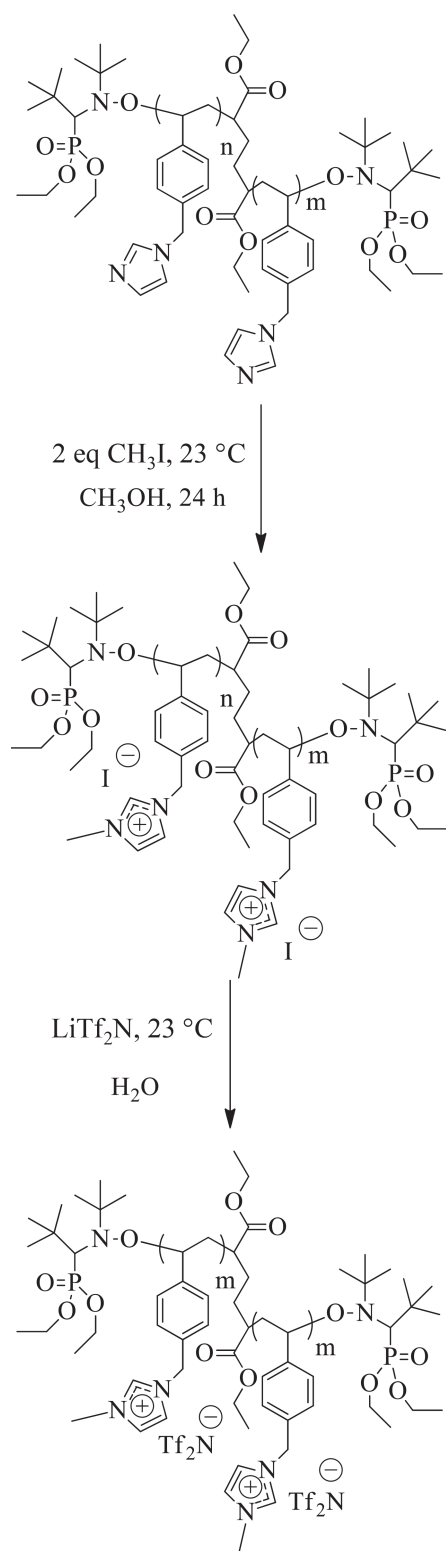
For triblock copolymers as efficient electromechanical membranes, ionic conductivity originates from the central block, which is positively charged poly(VBIm) with a mobile anion. The synthesis of poly(VBIm) was successfully reported in the earlier literature.<sup>[12,32,33]</sup> The molecular weight increased linearly with conversion with narrow PDIs throughout the polymerization of poly(VBIm). Ionic conductivity is a critical property for the application of these triblock copolymers in electromechanical membranes and the charged central block contributes to the ion transport in these triblock copolymer systems. The procedure for quaternization as reported in the earlier literature at 60 °C shown in Scheme 1 yielded bimodal distributions as observed in aqueous SEC and shown in Figure 1a. Therefore, quaternization conditions were probed at temperatures of 20, 40, and 60 °C.

As shown in Figure 1b,c, although bimodality disappeared at 20 °C, the % quaternization, as calculated from <sup>1</sup>H NMR, was low with 1-bromoethane. Thus, a more reactive alkylating agent, methyl iodide (CH<sub>3</sub>I), was used for quaternizing poly(VBIm) at 23 °C. Figure 1c shows that the PDI

remains narrow after quaternization with CH<sub>3</sub>I and also after anion exchange with Tf<sub>2</sub>N<sup>-</sup> (Scheme 2). Nitroxide links are prone to cleavage at higher temperatures due to the inherent instability of C–ON bond generating radicals. The observed high molecular weight is contributed to the radical–radical coupling reactions under the reflux conditions at high temperatures (between 40 and 60 °C). Using a stronger alkylating agent (methyl iodide), it is possible to avoid reflux conditions and still obtain 100% quaternization. This supports the formation of a central block having narrow PDIs and similar molecular weights. The quantitative anion exchange was confirmed using <sup>1</sup>H NMR spectroscopy and X-ray photoelectron spectroscopy (XPS). An increase in molecular weight was observed upon chain extension VBIm, confirming the controlled nature of the polymerization (Figure 1d).

The kinetics of poly(MVBIm-Tf<sub>2</sub>N) chain extension with styrene (Scheme 3) were investigated using <sup>1</sup>H NMR spectroscopy to calculate molecular weights. SEC was not used to determine molecular weights due to insolubility issues in the SEC mobile phase. Figure 2a,b demonstrate the linear increase in molecular weight with conversion in a controlled fashion to obtain ABA triblock copolymers with polystyrene external blocks and a poly(MVBIm-Tf<sub>2</sub>N) central block.

Thermomechanical properties of these triblock copolymers were ideal for electromechanical actuator applications. The thermal properties depended on the presence of charge and counterion selection. As observed in the literature,<sup>[24,33]</sup> T<sub>g</sub> of the homopolymer poly(VBIm) increased from 105 to 126 °C after quaternization with methyl iodide and decreased to 22 °C after anion exchange to Tf<sub>2</sub>N<sup>-</sup>. TGA showed that thermal stability decreased after quaternization due to the more basic anion I<sup>-</sup> and increased after anion exchange to the less basic counteranion Tf<sub>2</sub>N<sup>-</sup>. Mahanthappa and co-workers<sup>[24]</sup> previously determined the degradation mechanism for imidazolium homopolymers with varying counteranion and alkyl substituents. Homopolymers with Tf<sub>2</sub>N<sup>-</sup> counteranion displayed single-step degradation, which was attributed to the main chain



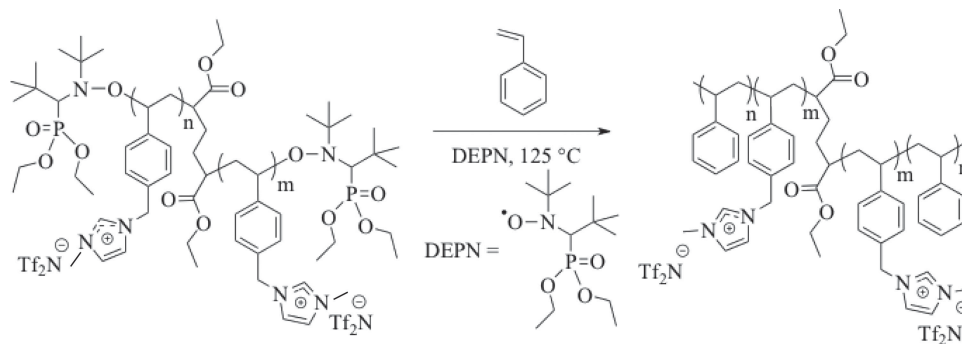
**Scheme 2.** Quaternization of poly(VBI<sub>m</sub>) using methyl iodide at 23 °C and subsequent anion exchange with LiTf<sub>2</sub>N.

polymer degradation. Table 1 shows the PDI remains narrow after quaternization with CH<sub>3</sub>I and anion exchange with LiTf<sub>2</sub>N. All triblock copolymers exhibited

two  $T_g$ s, corresponding to the quaternized central block and the second transition arose from the  $T_g$  of polystyrene as shown in Table 1. All triblock copolymers have high molecular weights and do not exhibit weight loss to 300 °C. <sup>1</sup>H NMR spectroscopy determined copolymer compositions, and Figure 2b shows the plot of the molecular weights also calculated using <sup>1</sup>H NMR spectroscopy versus monomer conversion.

The morphology of these triblock copolymers was investigated by indexing azimuthally integrated small-angle X-ray scattering (SAXS) profiles. In an effort to obtain higher degrees of long-range nanoscale order, samples for SAXS, DRS, and DMA were solvent-cast films from mixtures of 80:20 CHCl<sub>3</sub>:CH<sub>3</sub>OH and vacuum annealed for 5 d at 120 °C. Solvent cast films formed lamellae with long-range order and indicated a microphase-separated morphology. Figure 3 shows SAXS data for the triblock copolymer with 47 wt% styrene. The profile exhibits reflections at  $1q^*$ ,  $3q^*$ , and  $5q^*$  with structure factor extinctions of  $2q^*$  and  $4q^*$  where  $1q^*$  is the position of the primary scattering peak, indicating that the solvent cast films contained lamellae morphology with long-range order. The absence of peaks at  $2q^*$  and  $4q^*$  was due to structure factor extinctions at  $2q^*$  and  $4q^*$ . This indicates lamellar microstructure with symmetric volume fractions of each block.<sup>[34]</sup> The domain spacing of the lamellae was ca. 70 nm. This is the first time to observe microphase separation in these triblock copolymers as compared to earlier literature.<sup>[12]</sup> Wide-angle X-ray scattering (WAXS) shows peaks corresponding to correlation distances between amorphous carbon backbone chains, between phenyl groups and ionic aggregates in these triblock copolymers.

The interplay of ionic conductivity and membrane modulus is very critical for electromechanical transducer applications. All triblock copolymers displayed mechanical properties indicative of microphase separation as shown in Figure 4. The DMA  $T_g$ s, defined as the temperature where the modulus drops 1/2 of the glassy modulus, are 13, 9, and 6 °C for 20, 47, and 60 wt% styrene. DMA confirmed the presence of two distinct polymer phases with the central block  $T_g$  at ca. 10 °C and polystyrene external block  $T_g$  at 100 °C. Poly[Sty<sub>10</sub>-*b*-(MVBI<sub>m</sub>-Tf<sub>2</sub>N)<sub>80</sub>-*b*-Sty<sub>10</sub>], with 20 wt% polystyrene external blocks, had the highest DMA  $T_g$  of the central block without a  $T_g$  for the polystyrene external blocks, suggesting polystyrene in the ion-conducting phase. The room temperature modulus of ca. 100 MPa is ideal for actuator fabrication because this range affords a strong matrix for ion conduction without inhibiting actuation. Moisture content will also significantly influence electromechanical transducers, and chain extension with styrene resulted in an inherently more hydrophobic triblock copolymer. Charged polymers exhibit the ability to



**Scheme 3.** Synthesis of ABA triblock copolymer using DEPN at 125 °C poly[Sty-*b*-(MVBIm-Tf<sub>2</sub>N)-*b*-Sty] with polystyrene external blocks using nitroxide-mediated polymerization.

absorb moisture, which is quantified using TGA-sorption analysis.<sup>[35]</sup> These triblock copolymers showed less than 1% weight gain at 25 °C and 10% relative humidity over 10 h.

Ionic conductivity in single-ion conductors strongly depends on frequency and temperature.<sup>[36]</sup> The value of DC conductivity presented in Figure 5 is defined as the in-phase component of the conductivity, which is

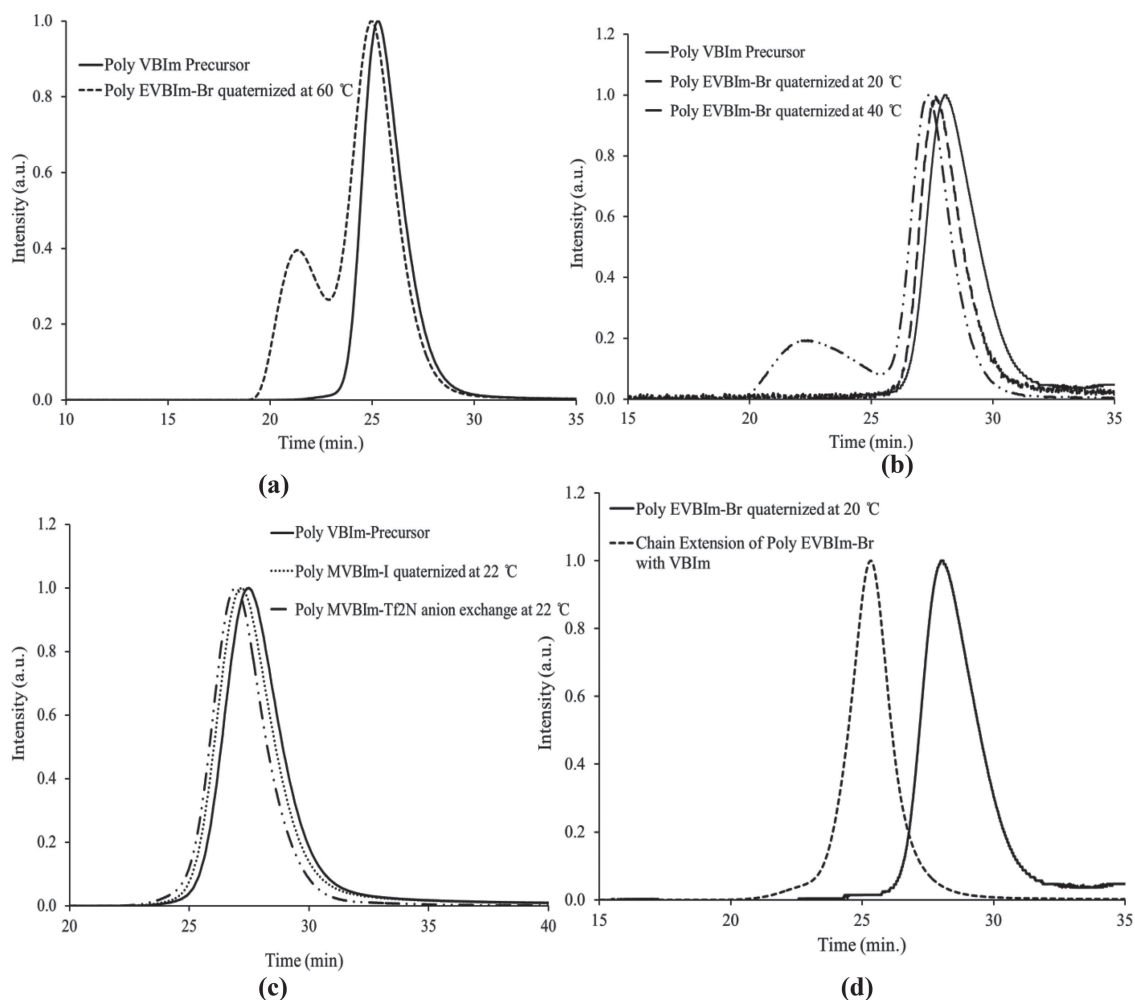


**Figure 1.** a) Bimodal peak observed in SEC after quaternization of poly(VBIIm) using 1-bromoethane at 60 °C. b) SEC traces of poly(VBIIm) and poly(EVBIIm-Br) obtained from different quaternization temperatures. c) SEC curves showing narrow PDI was maintained after quaternization of poly(VBIIm) with methyl iodide and anion exchange with LiTf<sub>2</sub>N. d) SEC traces of poly(EVBIIm-Br-20 °C) precursor and chain extended with VBIIm showing increase in molecular weight with conversion and narrow PDI.

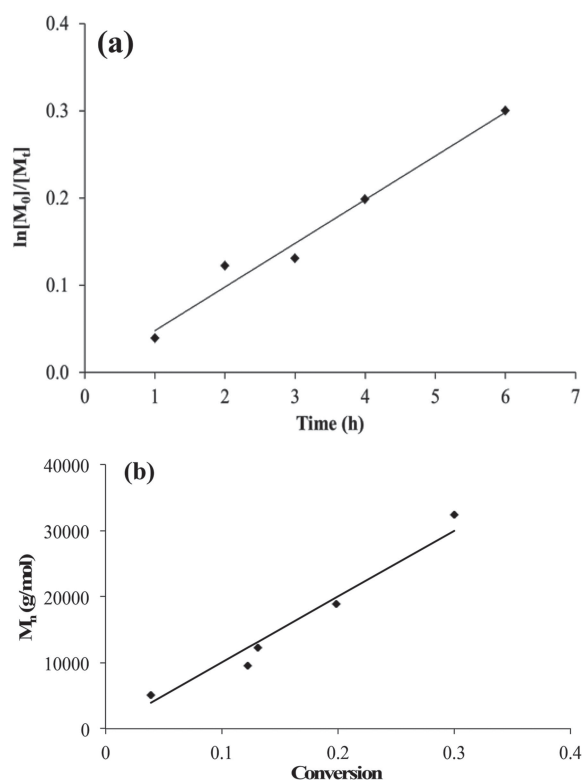


**Figure 2.** a) Monomer conversion  $\ln[M_0]/[M_t]$  vs time plot for chain extension of poly(MVBIIm-Tf<sub>2</sub>N) with styrene demonstrates pseudo-first-order kinetics.  $[M_0]$  and  $[M_t]$  represent the initial and instantaneous monomer concentrations at time  $t = 0$  and time  $t$  respectively. Solid line shows the linear increase in monomer conversion with time. b) Plot of number-average molecular weight ( $\bar{M}_n$ ) vs monomer conversion ( $[M_0]/[M_t]$ ) for chain extension of poly(MVBIIm-Tf<sub>2</sub>N) with styrene. The solid line represents the ideal molecular weight formation for a controlled radical polymerization.

independent of frequency in a roughly three-decade frequency range. Poly[Sty<sub>40</sub>-*b*-(MVBIIm-Tf<sub>2</sub>N)<sub>35</sub>-*b*-Sty<sub>40</sub>], which has the lowest weight percent of the ion-conducting blocks, exhibited the highest ionic conductivity and the lowest  $T_g$  of the ion-conducting block. Ionic conductivity decreased with increasing weight percent of

**Table 1.** Thermal transitions and molecular weights of imidazole-containing polymers.

Polymer	$\bar{M}_n$ [g mol <sup>-1</sup> ]	$\bar{M}_w^a$ [g mol <sup>-1</sup> ]	PDI <sup>a)</sup>	$T_{g1}^c$ [°C]	$T_{g2}^c$ [°C]	$T_{d,5\%}^d$ [°C]
Poly(VBIIm)	73 000 <sup>a)</sup>	73 400	1.13	105	–	348
Poly(MVBIIm-I)	77 000 <sup>a)</sup>	94 000	1.16	126	–	251
Poly(MVBIIm-Tf <sub>2</sub> N)	80 000 <sup>a)</sup>	99 000	1.17	22	–	339
Poly[Sty <sub>10</sub> -MVBIIm-Tf <sub>2</sub> N <sub>80</sub> -Sty <sub>10</sub> ]	100 000 <sup>b)</sup>	–	–	22	–	323
Poly[Sty <sub>35</sub> -MVBIIm-Tf <sub>2</sub> N <sub>80</sub> -Sty <sub>35</sub> ]	150 000 <sup>b)</sup>	–	–	27	106	329
Poly[Sty <sub>40</sub> -MVBIIm-Tf <sub>2</sub> N <sub>35</sub> -Sty <sub>40</sub> ]	200 000 <sup>b)</sup>	–	–	13	102	334

<sup>a)</sup>SEC: 35 °C, 1 mL min<sup>-1</sup>, MALLS detector, 54/23/23 (v/v/v%) H<sub>2</sub>O/CH<sub>3</sub>OH/AcOH, 0.1 M NaOAc;  $dn/dc = 0.2310$  mL g<sup>-1</sup>; <sup>b)</sup><sup>1</sup>H NMR spectroscopy: 400 MHz, DMSO-d<sub>6</sub>, 25 °C; <sup>c)</sup>DSC: 10 °C min<sup>-1</sup>, N<sub>2</sub> atmosphere, second heat; <sup>d)</sup>TGA: 10 °C min<sup>-1</sup>, N<sub>2</sub> atmosphere.

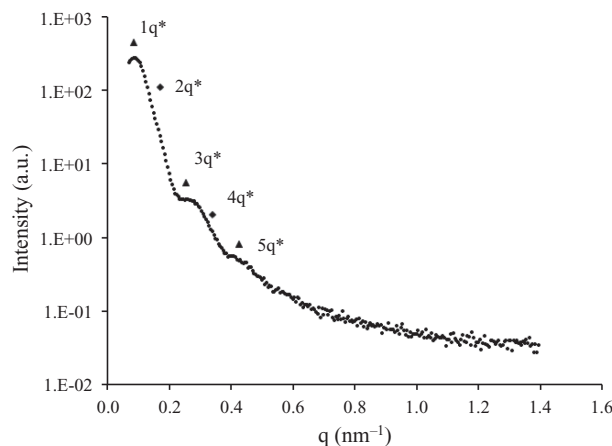


**Figure 3.** Small-angle X-ray scattering (SAXS) profile of charged poly[Sty<sub>35</sub>-*b*-(MVBIIm-Tf<sub>2</sub>N)<sub>80</sub>-*b*-Sty<sub>35</sub>] triblock copolymer having 47 wt% of styrene.

the imidazolium ion-containing block and correlated closely with the  $T_g$  of the ion-containing block except for poly[Sty<sub>10</sub>-*b*-(MVBIIm-Tf<sub>2</sub>N)<sub>80</sub>-*b*-Sty<sub>10</sub>], where an unusual Arrhenius temperature dependence of ionic conductivity was observed, and DMA suggested incorporation of polystyrene into the ion-conducting phase.

The ionic conductivity ( $\sigma$ ) can be simply expressed by:

$$\sigma = pe\mu \quad (1)$$

where  $p$ ,  $e$ , and  $\mu$  are total number density of conducting ions, elementary electric charge, and conducting ion mobility, respectively. It is crucial to determine whether the increase in ionic conductivity has a larger contribution from the number density of simultaneously conducting ions or their mobility in order to understand the anionic counterion conduction. This is assessed with EP at very low frequencies in DRS.<sup>[36]</sup>

In DRS, a sinusoidal ac field is applied to a thin-film sample sandwiched between two blocking electrodes. The EP occurs at frequencies low enough such that the transporting ions have sufficient time to polarize at the electrodes during each cycle. A physical model of EP,<sup>[37–40]</sup>

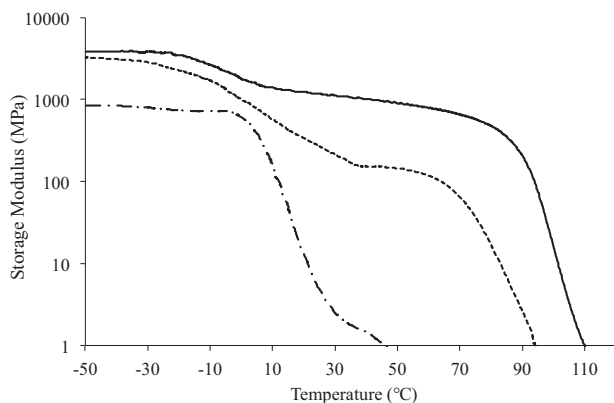


Figure 4. Thermomechanical properties of triblock copolymer poly[Sty-*b*-(MVBIm-Tf<sub>2</sub>N)-*b*-Sty] with a) 20 b) 47 and c) 60 wt% fractions of polystyrene blocks.

which has been applied to a number of single-ion conductors recently,<sup>[2,3,36,41–44]</sup> determined the number density of simultaneous conductors and their mobility. The time scale for full polarization at the electrode is:

$$\tau_{EP} \equiv \frac{\epsilon_{EP} \epsilon_0}{\sigma_{DC}} \quad (2)$$

where  $\epsilon_{EP}$  is the effective permittivity after the EP is complete,  $\epsilon_0$  is the permittivity of vacuum, and  $\sigma_{DC}$  is the DC conductivity. The time scale of conduction or when the ion motion becomes diffusive is:

$$\tau_{\sigma} \equiv \frac{\epsilon_s \epsilon_0}{\sigma_{DC}} \quad (3)$$

where  $\epsilon_s$  is the static dielectric constant. EP is regarded as a simple Debye relaxation in the Macdonald and Coelho model<sup>[37–40]</sup> with the loss tangent peak expressed as:

$$\tan \delta = \frac{\epsilon''}{\epsilon'} = \frac{\omega \tau_{EP}}{1 + \omega^2 \tau_{\sigma} \tau_{EP}} \quad (4)$$

where the peak maximum frequency relates to the geometric mean of the two fitting parameters  $\tau_{EP}$  and  $\tau_{\sigma}$ , demonstrated in Figure 6.

Since one type of ion is attached to the polymer chain and assumed to be immobilized, the counterion's mobility  $\mu$  and number density of simultaneous conducting ions  $p$  are then determined from the fitting parameters:

$$\mu = \frac{eL^2 \tau_{\sigma}}{4 \tau_{EP}^2 kT} \quad (5)$$

$$p = \frac{\sigma_{DC}}{e\mu} = \frac{4 \sigma_{DC} \tau_{EP}^2 kT}{e^2 L^2 \tau_{\sigma}} \quad (6)$$

where  $L$  is the sample thickness between electrodes,  $k$  is Boltzmann's constant, and  $T$  is the absolute temperature.

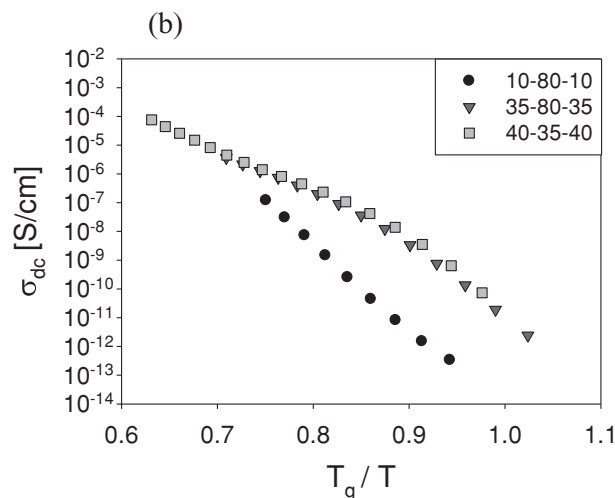
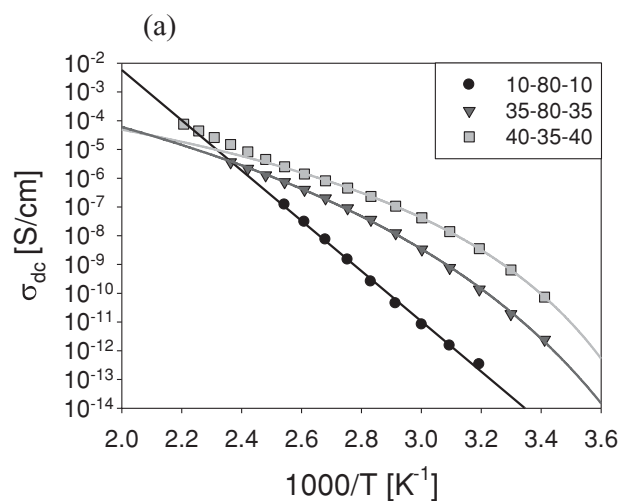


Figure 5. a) Temperature dependence of ionic conductivity for poly[Sty-*b*-(MVBIm-Tf<sub>2</sub>N)-*b*-Sty] having different weight percent of the styrene external blocks. The solid curves represent Equation 8 plotted with the parameters in Table 2. b) Ionic conductivity with respect to inverse temperature normalized by  $T_{g1}$  in Table 1.

The temperature dependence of the number density of simultaneously conducting ions calculated from Equation 6 is plotted in Figure 7 and is well-described using the Arrhenius equation:

$$p = p_{\infty} \exp\left(-\frac{E_a}{RT}\right) \quad (7)$$

where  $p_{\infty}$  is the conducting ion concentration as  $T \rightarrow \infty$  and  $E_a$  is the activation energy for conducting ions listed in Table 2. The activation energy is related to the Coulomb energy of a cation–anion pair, and this electrostatic attraction is the main driving force for pair and aggregate formation, mediated by an effective dielectric constant of the ion-conducting block.

The Arrhenius temperature dependence of the conducting ion concentration suggests the conducting

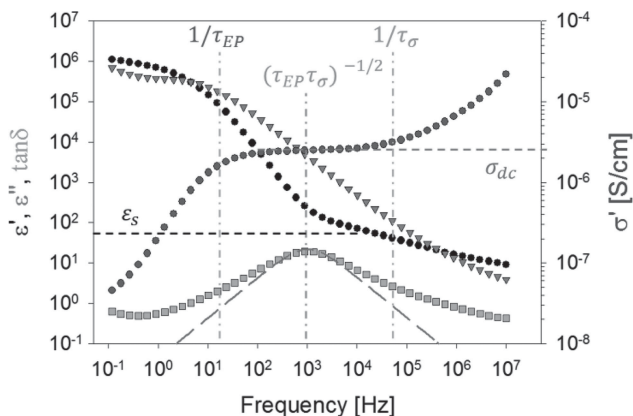


Figure 6. Dielectric spectra and fitting of the loss tangent peak with Equation 4 for Poly[Sty<sub>40</sub>-*b*-(MVBIm-Tf<sub>2</sub>N)<sub>35</sub>-*b*-Sty<sub>40</sub>] at 120 °C.

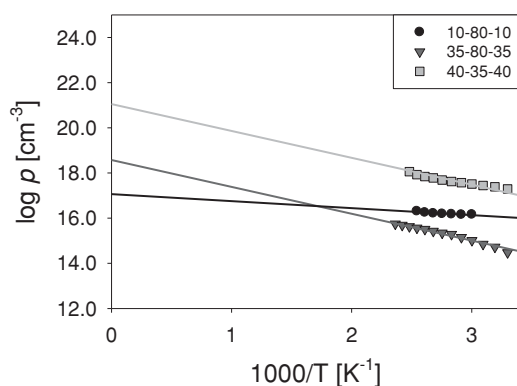


Figure 7. Temperature dependence of number density of simultaneously conducting ions for poly[Sty-*b*-(MVBIm-Tf<sub>2</sub>N)-*b*-Sty] having different weight percent of the styrene external blocks.

ions would be fully dissociated at infinite temperature. Poly[Sty<sub>40</sub>-*b*-(MVBIm-Tf<sub>2</sub>N)<sub>35</sub>-*b*-Sty<sub>40</sub>] has the highest number density of simultaneously conducting ions in the temperature range of DRS measurement, and the intercept of the Arrhenius fit of this sample in Figure 7 is fixed to  $p_0$ , calculated from a group contribution method with stoichiometry determined from the chemical structure.<sup>[45,46]</sup> Since all three ionomers have the same cation and mobile anion species, the activation energy (the slope in Figure 7), related to the coulomb energy between an ion pair, should be identical. Thus, the conducting ion concentration

Table 2. Fitting parameters (Equation 7) for the temperature dependence of the number density of simultaneously conducting ions.

Sample	$\log p_0$ [cm <sup>-3</sup> ]	$\log p_0$ [cm <sup>-3</sup> ]	$E_a$ [kJ mol <sup>-1</sup> ]	$p_\infty/p_0$
10-80-10	21.23	17.1	6.0	$7.4 \times 10^{-5}$
35-80-35	21.28	18.6	23	0.0021
40-35-40	21.05	21.05	23	1

Table 3. Fitting parameter (Equation 8) for the temperature dependence of ionic conductivity. Fitting parameter (Equation 8) for the temperature dependence of ionic conductivity.

Sample	$e\mu_\infty p_\infty$ [S cm <sup>-1</sup> ]	$D$	$T_0$ [K]	$E_a$ [kJ mol <sup>-1</sup> ]	$\sigma_{DC}$ at $T_g$ [S cm <sup>-1</sup> ]
10-80-10	$1.6 \times 10^{+15}$	0	NA	170	$4.3 \times 10^{-15}$
35-80-35	$4.8 \times 10^{-1}$	9.4	205	23	$1.2 \times 10^{-11}$
40-35-40	$2.2 \times 10^{-2}$	4.5	227	23	$1.1 \times 10^{-11}$

of poly[Sty<sub>35</sub>-*b*-(MVBIm-Tf<sub>2</sub>N)<sub>80</sub>-*b*-Sty<sub>35</sub>] is fitted with the slope fixed to be the same with poly[Sty<sub>40</sub>-*b*-(MVBIm-Tf<sub>2</sub>N)<sub>35</sub>-*b*-Sty<sub>40</sub>] and reveals a much smaller ratio of  $p_\infty/p_0$ , which represents the fraction of counterions that are participating in conduction. However, the number density of simultaneously conducting ions for poly[Sty<sub>10</sub>-*b*-(MVBIm-Tf<sub>2</sub>N)<sub>80</sub>-*b*-Sty<sub>10</sub>] is independent of temperature that corresponds to  $p_\infty \ll p_0$ , suggesting the majority of the counterions are trapped and unable to participate in conduction. Since ionic conductivity is obtained over a much wider temperature range than the EP model allows, the activation energies obtained from the Arrhenius fit to the number density of simultaneously conducting ions in Table 2 are used for poly[Sty<sub>35</sub>-*b*-(MVBIm-Tf<sub>2</sub>N)<sub>80</sub>-*b*-Sty<sub>35</sub>] and poly[Sty<sub>40</sub>-*b*-(MVBIm-Tf<sub>2</sub>N)<sub>35</sub>-*b*-Sty<sub>40</sub>] to fit the temperature dependence of ionic conductivity with:

$$\sigma_{DC} = e\mu_\infty p_\infty \exp\left(-\frac{DT_0}{T-T_0}\right) \exp\left(-\frac{E_a}{RT}\right) \quad (8)$$

where  $\mu_\infty$ ,  $T_0$ , and  $D$ , listed in Table 3, are, respectively, the highest temperature limit of mobility, the Vogel temperature, and the strength parameter that is reciprocally related to the fragility.

Poly[Sty<sub>10</sub>-*b*-(MVBIm-Tf<sub>2</sub>N)<sub>80</sub>-*b*-Sty<sub>10</sub>] shows Arrhenius-like temperature behavior of the ionic conductivity in Figure 5 that has also been observed in some polymerized ionic liquid systems,<sup>[47,48]</sup> suggesting the ion transport does not solely depend on the segmental motion of the ionomer. Thus, the temperature dependence of ionic conductivity for poly[Sty<sub>10</sub>-*b*-(MVBIm-Tf<sub>2</sub>N)<sub>80</sub>-*b*-Sty<sub>10</sub>] and was fitted to Equation 8 with  $D$  fixed to 0 to reveal a much larger activation energy than the other two triblock copolymers, 96% comes from mobility. The temperature dependence of the counterion's mobility calculated from Equation 5 is plotted in Figure 8. The ion mobility is fitted to the Vogel-Fulcher-Tammann (VFT) equation:

$$\mu = \mu_\infty \exp\left(-\frac{DT_0}{T-T_0}\right) \quad (9)$$

with the parameters  $D$  and  $T_0$  determined in the fitting of Equation 8. Data for poly[Sty<sub>10</sub>-*b*-(MVBIm-Tf<sub>2</sub>N)<sub>80</sub>-*b*-Sty<sub>10</sub>]

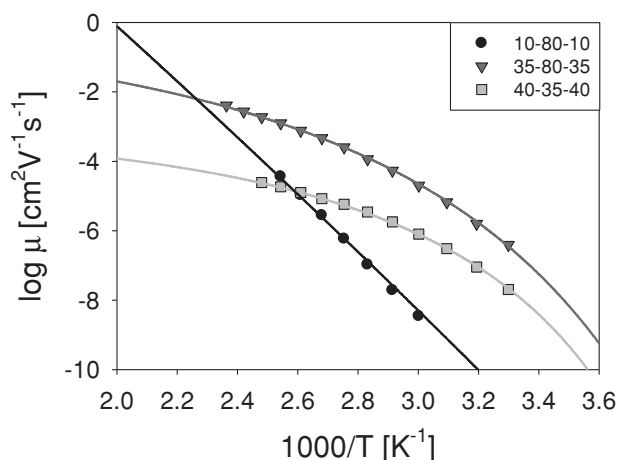


Figure 8. Temperature dependence of counterion's mobility for poly[Sty-*b*-(MVBIm-Tf<sub>2</sub>N)-*b*-Sty] having different weight percent of the styrene external blocks.

as the exception is fitted with Arrhenius temperature dependence.

The VFT temperature dependence indicates the coupling of ion transport to segmental motion of the polymer, except for poly[Sty<sub>10</sub>-*b*-(MVBIm-Tf<sub>2</sub>N)<sub>80</sub>-*b*-Sty<sub>10</sub>] where both ionic conductivity and ion mobility exhibit Arrhenius temperature dependence. Arrhenius temperature dependence of mobility suggests the poly[Sty<sub>10</sub>-*b*-(MVBIm-Tf<sub>2</sub>N)<sub>80</sub>-*b*-Sty<sub>10</sub>] sample has ion motion disconnected from polymer segmental motion, but this sample also shows the lowest conductivity. Poly[Sty<sub>35</sub>-*b*-(MVBIm-Tf<sub>2</sub>N)<sub>80</sub>-*b*-Sty<sub>35</sub>] has the highest ion mobility, with mostly contributions from a very small counterion fraction that are not trapped in ionic aggregates. Thus, ionic conductivity remained low because the fraction of ions contributing to conductivity was merely 0.2% if 100% for poly[Sty<sub>40</sub>-*b*-(MVBIm-Tf<sub>2</sub>N)<sub>35</sub>-*b*-Sty<sub>40</sub>].

The static dielectric constant  $\epsilon_s$ , shown in Figure 9a is calculated from  $\tau_\sigma$  in Equation 3 and defined as the low-frequency plateau of the dielectric constant  $\epsilon'(\omega)$  before EP begins.

Poly[Sty<sub>40</sub>-*b*-(MVBIm-Tf<sub>2</sub>N)<sub>35</sub>-*b*-Sty<sub>40</sub>] has the highest static dielectric constant and is much more polar than the other two triblock copolymers, where the ions are highly aggregated and dipoles cancel. This agrees with the number density of simultaneously conducting ions where poly[Sty<sub>40</sub>-*b*-(MVBIm-Tf<sub>2</sub>N)<sub>35</sub>-*b*-Sty<sub>40</sub>] has the largest fraction of ions contributing to conduction and also the highest ionic conductivity. The temperature dependence of static dielectric constant of all three triblock copolymers does not obey the Onsager prediction where thermal randomization of dipoles results in  $\epsilon_s$  inversely proportional to temperature and is only applicable to segments with polar groups in the liquid state where their motion is unrestricted by neighbors (far above  $T_g$ ). The static

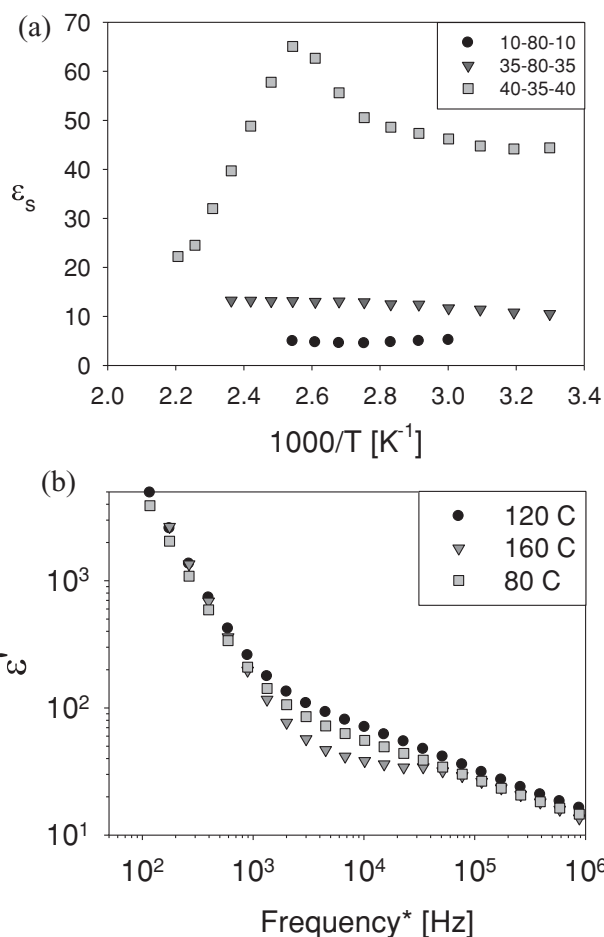


Figure 9. a) Temperature dependence of static dielectric constant for poly[Sty-*b*-MVBIm-Tf<sub>2</sub>N-*b*-Sty] having different weight percent of the styrene external blocks. b) Frequency dependence of dielectric permittivity  $\epsilon'$  for poly[Sty<sub>40</sub>-*b*-(MVBIm-Tf<sub>2</sub>N)<sub>35</sub>-*b*-Sty<sub>40</sub>] at 80, 120, and 160 °C. The data are shifted to align the low frequency EP part for comparison of  $\epsilon_s$ , usually defined as the value of  $\epsilon'$  before EP starts.

dielectric constant of poly[Sty<sub>40</sub>-*b*-(MVBIm-Tf<sub>2</sub>N)<sub>35</sub>-*b*-Sty<sub>40</sub>] starts to decrease at 120 °C ( $T_{g2} + 20$  °C), where cooling toward the  $T_g$  of the styrene microphase ( $T_{g2}$ ) restricts the motion of the neighboring molecules and limits the rotation/alignment of the dipoles in the ion-conducting microphase under an applied field. The decrease of  $\epsilon_s$  with decreasing temperature was also observed for poly(alkyl methacrylates) starting near  $T_g$ <sup>[49,50]</sup>; same behavior of  $\epsilon_s$  observed in polyacetaldehyde has been associated to an order-disorder transition controlling intermolecular orientation.<sup>[51]</sup> The very low  $\epsilon_s \approx 5$  for poly[Sty<sub>10</sub>-*b*-(MVBIm-Tf<sub>2</sub>N)<sub>80</sub>-*b*-Sty<sub>10</sub>] was consistent with ion motion decoupled from polymer segmental motion as the coulomb interaction between the pendant imidazolium and mobile anion dominate in the low  $\epsilon_s$  limit.

The actuation performance of these triblock copolymers without ionic liquid was previously reported in the

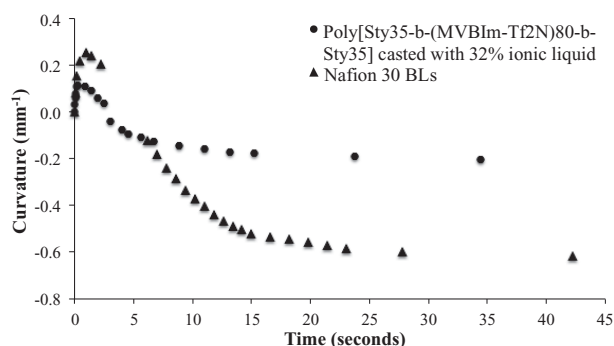


Figure 10. Curvature observed under a 4 V applied voltage for electromechanical actuators made from poly(Sty<sub>35</sub>-b-(MVBIm-Tf<sub>2</sub>N)<sub>80</sub>-b-Sty<sub>35</sub>) triblock copolymer cast with 32% of ionic liquid and Nafion membrane swollen with 34% ionic liquid.

literature and showed ion migration and accumulation at one electrode.<sup>[12]</sup> In the present study, triblock copolymer poly(Sty<sub>35</sub>-b-(MVBIm-Tf<sub>2</sub>N)<sub>80</sub>-b-Sty<sub>35</sub>) cast with 32 weight percent ionic liquid was fabricated into electromechanical actuators. A cast-with method ensured uniform incorporation of the IL throughout the triblock copolymer.<sup>[11]</sup> In the evaluation, a 4 V DC step input was applied to the actuator at ambient conditions (20 °C and ca. 43% RH) and a high definition camera for further analysis recorded the induced electromechanical actuation. The analysis demonstrated electromechanical actuation upon application of low voltages (Figures 10 and 11), which is the first time these triblock copolymers have demonstrated actuation. A common feature for electroactive devices containing ionic liquids is a bidirectional bending behavior caused by accumulation of a charged species at one electrode followed by slower accumulation of the opposite charged species at the opposite electrode,<sup>[31]</sup> as is observed in

Figure 11. The free ions (cations in Nafion and anions in the reported polymer) did contribute to the bending but their effect is highly limited, due to its much smaller size and amount as compared to the ions of the ionic liquid. Our group has reported the bending performance of the actuator made of “dry” membrane of another cationic imidazolium-containing polymer, where only one direction bending is observed as a result of the transportation and accumulation of counteranions only. The membranes (both Nafion and reported polymer) in the current study mainly act as a “container” of ionic liquid, and provide channels for the migration of the ions of ionic liquid. We propose the ions of the ionic liquid are dominating the bending performance of the actuators within this study. These triblock copolymers exhibited electrochemically stability between +4 and -4 V observed through cyclic voltammetry.

The bending performance of the actuator of the poly(Sty<sub>35</sub>-b-(MVBIm-Tf<sub>2</sub>N)<sub>80</sub>-b-Sty<sub>35</sub>) triblock copolymer membrane, and a Nafion membrane swollen with 32% ionic liquid as control are shown in Figure 10. Due the different size and migration speed of the cation and anion of IL in the actuator, the triblock copolymer actuator experienced the same bidirectional bending behavior as the Nafion actuator<sup>[31]</sup> under the 4 V DC applied voltage. Although the triblock copolymer actuator showed smaller bending curvature as compared to Nafion, the actuation speed was fairly rapid and comparable to the Nafion actuator. The fast actuation speed indicates the triblock copolymer had good ion conductivity, while the smaller bending curvature was presumably due to lower IL uptake. The calculations of the IL uptake are slightly different for these two cases because of the different fabrication process. The uptake of the reported polymer is for the membrane only

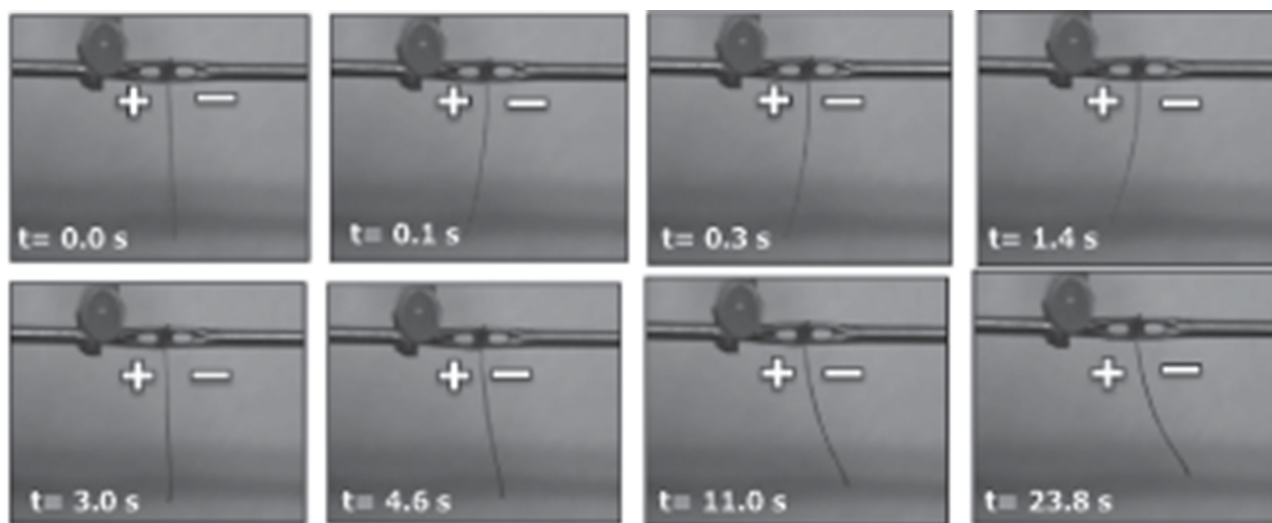


Figure 11. Still images of electromechanical transducer fabricated from poly(Sty<sub>35</sub>-b-(MVBIm-Tf<sub>2</sub>N)<sub>80</sub>-b-Sty<sub>35</sub>) film cast with 32 wt% ionic liquid [EMIm] [TfO] under applied potential of 4 V.

while the Nafion is for the membrane plus CNC layer. As a result, although the uptake of Nafion (34%) seems just slightly higher than the one of the reported polymer (32%), the net amount of the IL in the Nafion should be clearly higher than in the reported polymer.

#### 4. Conclusion

A series of well-defined ABA triblock copolymers, poly[Sty-*b*-(MVBIm-Tf<sub>2</sub>N)-*b*-Sty], with different compositions of central and external blocks were synthesized using NMP. These are microphase-separated triblock copolymers, exhibiting good mechanical stability and well-defined structure as observed using DMA and SAXS, respectively. For the first time, a detailed study of ion transport in these triblock copolymers was performed using DRS to understand the contributions of mobile ion concentration, static dielectric constant, and ionic mobility. Poly(Sty<sub>40</sub>-*b*-(MVBIm-TF<sub>2</sub>N)<sub>35</sub>-*b*-Sty<sub>40</sub>) (47 wt% styrene external blocks) exhibited a VFT temperature dependence of ionic conductivity and mobility, indicating coupling between ionic conductivity and segmental motion. This triblock copolymer also displayed the highest ionic conductivity, mobile ion concentration, and static dielectric constant of the triblock copolymers studied. When cast with 32 wt% ionic liquid, poly(Sty<sub>40</sub>-*b*-(MVBIm-Tf<sub>2</sub>N)<sub>35</sub>-*b*-Sty<sub>40</sub>) showed actuation for the first time in the literature.

#### Supporting Information

Supporting Information is available from the Wiley Online Library or from the author. Synthesis, X-ray photoelectron spectroscopy, TGA-sorption analysis, wide-angle X-ray scattering, and cyclic voltammetry data are available.

**Acknowledgements:** This material is based on work supported by the U.S. Army Research Laboratory and the U.S. Army Research Office under contract/grant number W911NF-07-1-0452 Ionic Liquids in Electro-Active Devices Multidisciplinary University Research Initiative (ILEAD MURI). The authors acknowledge the Laboratory for Research on the Structure of Matter at Penn (MRSEC NSF DMR11-20901) for instrument support.

Received: March 2, 2014; Revised: April 26, 2014;  
Published online: May 26, 2014; DOI: 10.1002/mcp.201400121

**Keywords:** actuators; membranes; nitroxide-mediated polymerization

- [1] A. J. Duncan, D. J. Leo, T. E. Long, *Macromolecules* **2008**, *41*, 7765.  
[2] G. J. Tudryn, W. Liu, S.-W. Wang, R. H. Colby, *Macromolecules* **2011**, *44*, 3572.

- [3] S.-W. Wang, W. Liu, R. H. Colby, *Chem. Mater.* **2011**, *23*, 1862.  
[4] B. J. Akle, M. D. Bennett, D. J. Leo, K. B. Wiles, J. E. McGrath, *J. Mater. Sci.* **2007**, *42*, 7031.  
[5] B. J. Akle, D. J. Leo, *Smart Mater. Struct.* **2007**, *16*, 1348.  
[6] Y. Bar-Cohen, Q. Zhang, *MRS Bull.* **2008**, *33*, 173.  
[7] I.-S. Park, K. Jung, D. Kim, S.-M. Kim, K. J. Kim, *MRS Bull.* **2008**, *33*, 190.  
[8] R. Montazami, S. Liu, Y. Liu, D. Wang, Q. Zhang, J. R. Heflin, *J. Appl. Phys.* **2011**, *109*, 104301.  
[9] M. D. Green, J.-H. Choi, K. I. Winey, T. E. Long, *Macromolecules* **2012**, *45*, 4749.  
[10] S. Liu, R. Montazami, Y. Liu, V. Jain, M. Lin, J. R. Heflin, Q. Zhang, *Appl. Phys. Lett.* **2009**, *95*, 023505.  
[11] T. Wu, D. Wang, M. Zhang, J. R. Heflin, R. B. Moore, T. E. Long, *Appl. Mater. Int.* **2012**, *4*, 6552.  
[12] M. D. Green, D. Wang, S. T. Hemp, J.-H. Choi, K. I. Winey, J. R. Heflin, T. E. Long, *Polymer* **2012**.  
[13] S. Nemat-Nasser, J. Y. Li, *J. Appl. Phys.* **2000**, *87*, 3321.  
[14] L. M. Weiland, D. J. Leo, *Smart Mater. Struct.* **2004**, *13*, 323.  
[15] A. J. Duncan, D. J. Leo, T. E. Long, B. J. Akle, J. K. Park, R. B. Moore, in *16th Int. Symp. Smart Structures and Materials & Nondestructive Evaluation and Health Monitoring*, International Society for Optics and Photonics, **2009**, p 728711.  
[16] J. Lin, Y. Liu, Q. Zhang, *Polymer* **2011**, *52*, 540.  
[17] A. Eisenberg, B. Hird, R. Moore, *Macromolecules* **1990**, *23*, 4098.  
[18] K. A. Mauritz, R. B. Moore, *Chem. Rev.* **2004**, *104*, 4535.  
[19] M. D. Green, C. Schreiner, T. E. Long, *J. Phys. Chem. A* **2011**, *115*, 13829.  
[20] S. Cheng, F. L. Beyer, B. D. Mather, R. B. Moore, T. E. Long, *Macromolecules* **2011**, *44*, 6509.  
[21] M. D. Green, D. Salas-de la Cruz, Y. Ye, J. M. Layman, Y. A. Elabd, K. I. Winey, T. E. Long, *Macromol. Chem. Phys.* **2011**, *212*, 2522.  
[22] R. L. Weber, Y. Ye, A. L. Schmitt, S. M. Banik, Y. A. Elabd, M. K. Mahanthappa, *Macromolecules* **2011**, *44*, 5727.  
[23] M. H. Allen Jr., S. Wang, S. T. Hemp, Y. Chen, L. A. Madsen, K. I. Winey, T. E. Long, *Macromolecules* **2013**, *46*, 3037.  
[24] R. L. Weber, Y. Ye, S. M. Banik, Y. A. Elabd, M. A. Hickner, M. K. Mahanthappa, *J. Polym. Sci., B: Polym. Phys.* **2011**, *49*, 1287.  
[25] Y. Ye, J.-H. Choi, K. I. Winey, Y. A. Elabd, *Macromolecules* **2012**, *45*, 7027.  
[26] B. D. Mather, J. R. Lizotte, T. E. Long, *Macromolecules* **2004**, *37*, 9331.  
[27] B. D. Mather, M. B. Baker, F. L. Beyer, M. A. Berg, M. D. Green, T. E. Long, *Macromolecules* **2007**, *40*, 6834.  
[28] S. Grimaldi, J.-P. Finet, F. Le Moigne, A. Zeghdou, P. Tordo, D. Benoit, M. Fontanille, Y. Gnanou, *Macromolecules* **2000**, *33*, 1141.  
[29] P. A. Heiney, *Comm. Powder Diffraction Newsletter* **2005**, *32*, 9.  
[30] S. Liu, S. Srinivasan, M. C. Grady, M. Soroush, A. M. Rappe, *J. Phys. Chem. A* **2012**, *11622*, 5337.  
[31] Y. Liu, S. Liu, J. Lin, D. Wang, V. Jain, R. Montazami, J. R. Heflin, J. Li, L. Madsen, Q. Zhang, *Appl. Phys. Lett.* **2010**, *96*, 223503.  
[32] Y. Ye, Y. A. Elabd, *Macromolecules* **2011**, *44*, 8494.  
[33] Y. Ye, Y. A. Elabd, *Polymer* **2011**, *52*, 1309.  
[34] R.-J. Roe, *Methods of X-ray and Neutron Scattering in Polymer Science*, Oxford University Press, New York **2000**.

- [35] M. H. Allen Jr., S. Wang, S. T. Hemp, Y. Chen, L. A. Madsen, K. I. Winey, T. E. Long, *Macromolecules* **2013**, *46*, 3037.
- [36] M. Lee, U. H. Choi, R. H. Colby, H. W. Gibson, *Chem. Mater.* **2010**, *22*, 5814.
- [37] J. R. Macdonald, *Phys. Rev.* **1953**, *92*, 4.
- [38] R. Coelho, *J. Non-Cryst. Solids* **1991**, *131*, 1136.
- [39] R. Coelho, *Rev. Phys. Appl.* **1983**, *18*, 137.
- [40] J. R. Macdonald, *Solid State Ionics* **2005**, *176*, 1961.
- [41] R. J. Klein, S. Zhang, S. Dou, B. H. Jones, R. H. Colby, J. Runt, *J. Chem. Phys.* **2006**, *124*, 144903.
- [42] D. Fragiadakis, S. Dou, R. H. Colby, J. Runt, *J. Chem. Phys.* **2009**, *130*, 064907.
- [43] D. Fragiadakis, S. Dou, R. H. Colby, J. Runt, *Macromolecules* **2008**, *41*, 5723.
- [44] U. H. Choi, M. Lee, S. Wang, W. Liu, K. I. Winey, H. W. Gibson, R. H. Colby, *Macromolecules* **2012**, *45*, 3974.
- [45] D. W. van Krevelen, K. te Nijenhuis, *Properties of Polymers: Their Correlation with Chemical Structure; Their Numerical Estimation and Prediction from Additive Group Contributions, 4th Ed.*, Elsevier Science, Amsterdam, The Netherlands **2009**.
- [46] J. M. Slattery, C. Daguene, P. J. Dyson, T. J. Schubert, I. Krossing, *Angew. Chem.* **2007**, *119*, 5480.
- [47] H. Chen, J.-H. Choi, D. Salas-de la Cruz, K. I. Winey, Y. A. Elabd, *Macromolecules* **2009**, *42*, 4809.
- [48] K. Nakamura, T. Saiwaki, K. Fukao, *Macromolecules* **2010**, *43*, 6092.
- [49] Y. Ishida, M. Matsuo, K. Yamafuji, *Kolloid-Z. Z. Polym.* **1962**, *180*, 108.
- [50] H. Sasabe, S. Saito, *J. Polym. Sci., Part B: Polym. Phys.* **1968**, *6*, 1401.
- [51] G. Williams, *Trans. Faraday Soc.* **1963**, *59*, 1397.